Soft Matter

PAPER

Cite this: *Soft Matter*, 2015, **11**, 5122

Collective dynamics of non-coalescing and coalescing droplets in microfluidic parking networks†

Swastika S. Bithi and Siva A. Vanapalli*

Received 5th May 2015,
Accepted 22nd May 2015

DOI: 10.1039/c5sm01077b

www.rsc.org/softmatter

We study the complex collective dynamics mediated by flow resistance interactions when trains of non-coalescing and coalescing confined drops are introduced into a microfluidic parking network (MPN). The MPN consists of serially connected loops capable of parking arrays of drops. We define parking modes based on whether drops park without breakage or drop fragments are parked subsequent to breakage or drops park after coalescence. With both non-coalescing and coalescing drops, we map the occurrence of these parking modes in MPNs as a function of system parameters including drop volume, drop spacing and capillary number. We find that the non-coalescing drops can either park or break in the network, producing highly polydisperse arrays. We further show that parking due to collision induced droplet break-up is the main cause of polydispersity. We discover that collisions occur due to a crowding instability, which is a natural outcome of the network topology. In striking contrast, with coalescing drops we show that the ability of drops to coalesce rectifies the volume of parked polydisperse drops, despite drops breaking in the network. We find that several parking modes act in concert during this hydrodynamic self-rectification mechanism, producing highly monodisperse drop arrays over a wide operating parameter space. We demonstrate that the rectification mechanism can be harnessed to produce two-dimensional arrays of microfluidic drops with highly tunable surface-to-volume ratios, paving the way for fundamental investigations of interfacial phenomena in emulsions.

I. Introduction

Microfluidic methods allow rapid generation of monodisperse emulsion droplets.[1,2] When a collection of such monodisperse droplets flow through linear microchannels[3,4] or a network of microchannels[5–7] complex collective phenomena can be manifested. The collective behavior results from long-range hydrodynamic interactions induced by either dipolar flow fields or hydrodynamic resistive coupling. Understanding the collective dynamics due to such interactions is important in microfluidic applications, for example to sort,[8] synchronize[9,10] or store[11–14] drops.

Recently, a unique class of microchannel networks called microfluidic parking networks (MPNs) have been reported that allow generation of two-dimensional arrays of drops called static drop arrays (SDAs).[11–15] As shown in Fig. 1, MPNs consist of a series of interconnected parking loops, where each parking loop has a bypass channel and a lower branch containing a fluidic trap. When a train of drops, similar in volume to the trap is introduced into the MPN, drops initially enter the low-resistance bypass channel influencing the decision of latter drops to enter the trap (see Fig. 1b); thus producing SDAs. The benefit of such SDAs is significant as many observations can be simultaneously recorded from an ensemble of spatially addressed drops. MPN-based SDAs have been used to investigate crystallization of proteins and inorganic materials,[16] and analyze cells.[17,18]

The fundamental basis for routing droplets in MPNs lies in the fact that when confined drops flow through interconnected channels, they act as fluidic resistors altering instantaneously the flow rate in branches, affecting the choices that drops make at junctions. Thus, although the trapping process in Fig. 1b appears efficient the dynamics can be far more complex. This is because, the instantaneous flow rate can be modulated by a number of variables including droplet characteristics (*e.g.* drop volume and spacing), flow conditions (*e.g.* capillary number) and network parameters (*e.g.* branch lengths and trap geometry), lending to a large control parameter space. Unraveling the collective behaviors as a function of system parameters is critical to robust production and manipulation of SDAs. However, studies to date have largely investigated collective dynamics due to droplet trains in microfluidic bifurcations[5,7,19–23] and ladder networks.[9,10,21,22,24]

Department of Chemical Engineering, Texas Tech University, Lubbock, TX 79409, USA. E-mail: siva.vanapalli@ttu.edu

† Electronic supplementary information (ESI) available. See DOI: 10.1039/c5sm01077b

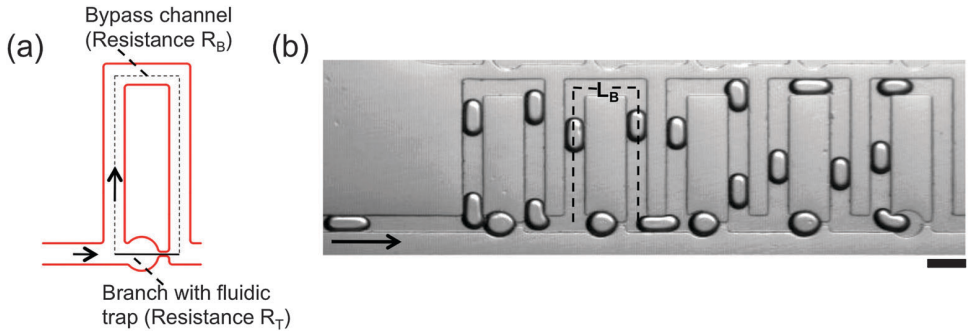

Fig. 1 (a) Schematic of a single microfluidic parking loop. The dashed line represents the bypass channel with path resistance R_B and the solid line represents the branch with fluidic trap with path resistance R_T. (b) A snapshot of the collective dynamics of non-coalescing drops in the microfluidic parking network. The dashed line indicates the length of the bypass (L_B). Arrow indicates flow direction. Q_o = 20 μL h^{-1} and Q_w/Q_o = 0.3. In this MPN, R_T/R_B = 1.5. Scale bar is 500 μm.

In a previous study, we focused on collective behaviors arising from changing the ratio of flow resistance of the trap to bypass channel (R_T/R_B) in MPNs.[13] Specifically, we observed that for R_T/R_B = 0.19 and 0.38 drops directly entered the trap channel and could be parked only at very low flow rates; otherwise they readily squeezed through the traps. The use of low flow rates also led to variability in drop volumes (*e.g.* 10–15% variation for flow rates below 10 μL h^{-1}) in the train due to pump fluctuations, affecting the monodispersity of the SDA. At R_T/R_B = 1.56, drops entered the bypass channels and trapping occurred similar to that shown in Fig. 1b. However, effective parking occurred under very limited flow conditions, and most of the behaviors were dominated by drop breakup and squeezing. Finally, at R_T/R_B = 4.38, we observed no parking of drops because all the drops went solely through the low-resistance bypass channels.

More recently, we showed that the ability of droplets to coalesce in MPNs can produce unexpected collective behaviors.[14] When producing microfluidic emulsions, the standard practice is to use sufficient surfactant in the continuous phase to prevent droplet coalescence.[25] In fact, prior studies on SDA production[11–13,18,26] also used non-coalescing drops to store droplets in MPNs. Contrary to this prevailing practice; we discovered that switching to trains of drops with little or no surfactant can display a stunning collective behavior called hydrodynamic self-rectification.[14] Unlike the non-coalescing drops, which can only park and/or fragment, this simple switch produces coalescing drops which can also merge with other drops in the network. As a result, incoming drops were observed to rectify the volume of trapped polydisperse drops through coalescence and subsequent detachment, yielding exceptionally monodisperse SDAs over a wide range of flow conditions.

Even though both surfactant-covered and surfactant-free droplets have been shown to produce droplet arrays, the collective dynamics is far more complex and several fundamental aspects remain to be understood. For example, individual events such as drop parking, break-up (by collision or extensional flow) and coalescence have been shown to occur in the network, but under what conditions of drop size, spacing and capillary number do these events occur remains unknown. Likewise two or more of these events are expected to occur in the network concurrently due to the collective nature of the dynamics, yet it is currently unclear for a given set of system parameters which event occurs more frequently and why. Addressing such fundamental aspects is crucial to achieving full control over individual drop volume in MPNs, which will enable production of microfluidic droplet arrays with highly tunable surface-to-volume ratios (*e.g.* big and small drops in the same array or arrays with gradually varying drop volumes).

In this study we define parking modes based on whether drops park without breakage or drop fragments are parked subsequent to breakage or drops park after coalescence – enabling us to correlate modes of parking with the individual trap volumes. Using this framework of parking modes we decode the complex dynamics in MPNs due to both non-coalescing (surfactant-coated) and coalescing (surfactant-free) drops. In contrast to prior works, the outcomes of this study are (i) identification of the system parameter space where different parking modes operate (ii) mechanistic insights into the parking modes and collective behaviors and (iii) knowledge of how different parking modes influence the degree of polydispersity of the SDA – which is a crucial parameter of interest for both fundamental investigations and applications. We conclude with a discussion on how coalescing droplets can be used to produce SDAs with high fidelity control over the volume of individual parked droplets.

II. Results

A. Collective dynamics of non-coalescing drops

To probe the collective dynamics due to non-coalescing drops, we introduced trains of surfactant-coated drops into the MPN by manipulating the aqueous (Q_w) and oil flow rates (Q_o) at an upstream T-junction. We note that the drop size, spacing and speed of the train are not independently controllable using T-junction geometry. Nevertheless, consistent with previous reports,[27] we find that the drop size increases with Q_w/Q_o and the drop spacing in the train increases as Q_o increases. All the experiments were conducted in a 60-trap MPN with R_T/R_B = 1.5, where we previously observed collective interactions to be

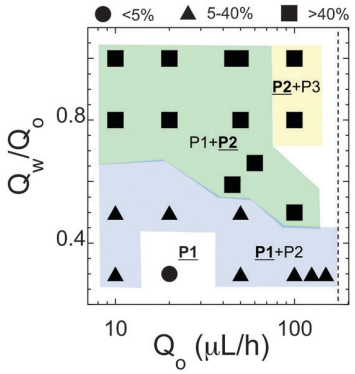

Fig. 2 The tested flow conditions for non-coalescing drops (2 wt% Span 80) and the associated polydispersity of trapped volumes is shown in the legend. The shaded areas show the modes of parking and letter in bold and underlined represent the dominate mode-white: P1, blue: P1 + P2, green: P1 + P2, yellow: P2 + P3 (see text for details). The dashed vertical line indicates the approximate onset of squeezing of the drops through the traps.

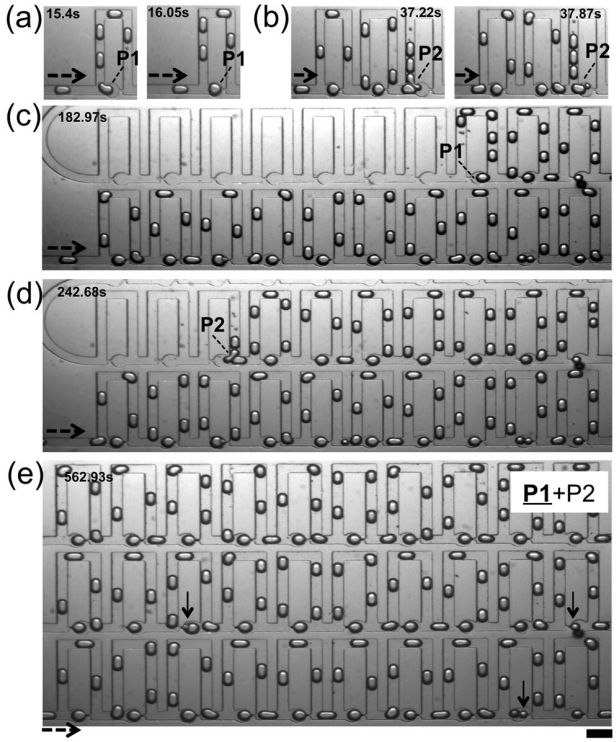

Fig. 3 Time-stamped image sequence showing the collective dynamics of non-coalescing drops in the MPN, when volume of primary drops in the train is comparable to the trap volume. (a, c) Images showing parking mode P1, where drops are captured in traps due to collective hydrodynamic feedback from drops in the bypass. (b, d) Images showing collision-induced parking mode P2 that leads to drop fragmentation. (e) Final polydisperse SDA resulting from occurrence of both parking modes P1 and P2 in the network. In the top right, P1 is bolded and underlined to indicate that P1 occurs more often than P2. The dashed arrows indicate the flow direction. The solid arrows indicate the fragmented drops due to P2 mode. Q_o = 10 μL h^{-1} and Q_w/Q_o = 0.5. Scale bar is 500 μm.

prominent.[13] The Reynolds number and capillary number were less than 0.01.

In Fig. 2, we show the measured polydispersity of the SDA at several combinations of the control parameters Q_w/Q_o and Q_o. Excluding the regime where drops squeeze through the fluidic trap at $Q_o > 150$ μL h^{-1} (see the dashed vertical line in Fig. 2), all other explored flow conditions lead to drop parking in the array. However, we find only one flow condition $-Q_o = 20$ μL h^{-1} and $Q_w/Q_o = 0.3$, where the SDA is monodisperse (polydispersity index is <5%). At all other flow conditions, the polydispersity index is ≥5% implying a significant non-uniformity in the size distribution of the trapped droplets. As shown in Fig. 3 and 4, the polydispersity is due to break-up of drops in the MPN.

1. Modes of parking. The sensitive dependence of polydispersity on the flow conditions is because of three different modes of drop parking manifested by collective interactions in the network. Below, we discuss these different modes of parking.

P1 – discrete drop parking. In this mode of parking, we find that drops get parked in the fluidic traps without breakage as shown in Fig. 3a and c. Because the hydrodynamic resistance of the bypass channel is lower, drops initially choose the bypass. If a specified number of drops are present in the bypass, the carrier fluid flow rate can be reduced to such an extent, that the subsequent drop enters the fluidic trap and is parked. Drops in the bypass therefore collectively induce a hydrodynamic feedback[7] on the incoming drop, modifying its decision to enter the bypass. At the flow condition of $Q_o = 20$ μL h^{-1} and $Q_w/Q_o = 0.3$, this mode of parking consistently occurred in each of the loop, generating monodisperse SDA.

P2 – drop parking due to collision-induced break-up. We observe that pairs of drops comparable in size to the trap, collide at the junctions and undergo break-up,[28] as shown in Fig. 3b and d. This parking mode often leaves the trap underfilled (see the arrows in Fig. 3e). Broken portions of the drops moving in the bypass introduce 'noise' in the collective hydrodynamic feedback causing drops not to fragment evenly at each junction and therefore degrading the uniformity of the trapped volumes in the array.

P3 – drop parking due to flow-induced break-up. When the confined drops in the train are larger than the trap size and the carrier fluid flow rate is high, a different parking mode emerges. We find that a portion of the drop enters the bypass channel before it fragments at the junction due to the elongational flow,[29,30] leaving a remnant in the trap (see Fig. 4a and c). Similar to parking mode P2, when this parking mode dominates, significant polydispersity is observed because the drop fragments in the bypass disrupt the collective hydrodynamic feedback necessary to break the large drops in the same volume ratio at each junction.

We often observe that two parking modes act in concert, with typically one mode occurring more frequently than the other. For example, for the experiment reported in Fig. 3, both P1 and P2 occur in the network with P1 occurring more often

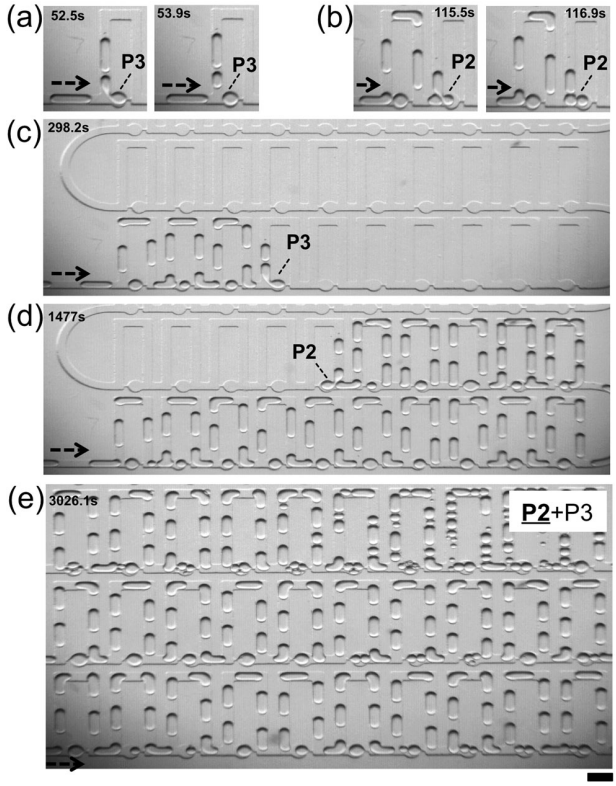

Fig. 4 Time-stamped image sequence showing the collective dynamics of non-coalescing drops in the MPN, when volume of primary drops in the train is larger than the trap volume. (a, c) Images showing parking mode P3, where drops are captured due to elongational flow-induced breakup of the primary drops. (b, d) Images showing collision-induced parking mode P2 that leads to drop fragmentation. (e) Final polydisperse SDA resulting from occurrence of both parking modes P2 and P3 in the network with P2 dominating the dynamics. Q_o = 100 μL h^{-1} and Q_w/Q_o = 0.8. The dashed arrows indicate the flow direction. Scale bar is 500 μm.

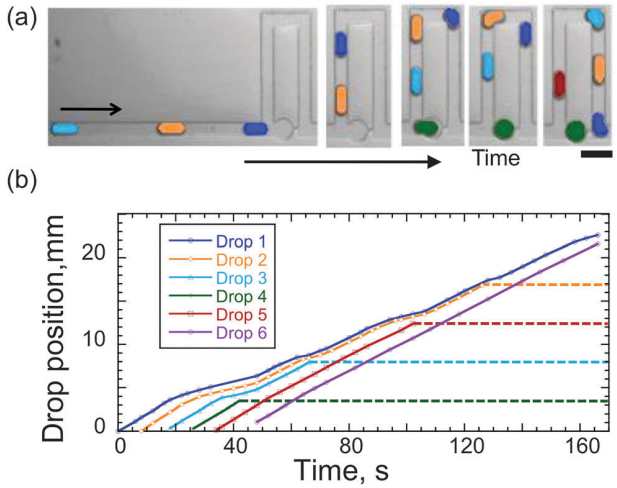

Fig. 5 Crowding of drops in the bypass channels in an MPN (a) images showing color-coded drops and (b) their corresponding location in the network as a function of time (bottom). Significant non-linear variations in droplet spacing are apparent. The horizontal dashed line indicates end of the trajectory due to droplet parking. Time zero is taken as when the first drop in the train arrives at the junction of the first loop in the network. The flow condition corresponding to (a) and (b) is Q_o = 20 μL h^{-1} and Q_w/Q_o = 0.3. Scale bar is 500 μm.

than P2. Likewise in Fig. 4, both P2 and P3 occur with P2 dominating the drop dynamics. Given that in Fig. 3 the non-breakup mode P1 dominates, the polydispersity of the array is significantly lower than that shown in Fig. 4.

2. **Mechanism promoting droplet collisions.** In Fig. 2, we show the different parking modes that occur at each of the tested flow conditions. We find that the P2 mode *i.e.* drop parking due to collision-induced breakup, manifests itself in majority of the experiments, and dominates the dynamics at several flow conditions. We therefore asked what mechanism could have led to collisions between drops, even though they enter into the MPN well separated. To elucidate the mechanism, we examined in detail the collective dynamics of drops at the singular flow condition where there were no break-up events *i.e.* at Q_o = 20 μL h^{-1} and Q_w/Q_o = 0.3. We tracked the first six drops in the train as shown in Fig. 5a and plot their trajectories in Fig. 5b, where the vertical distance between any two trajectories represents the interdrop spacing at a given time, and flattening of the trajectory indicates droplet parking. We also computed the local slope of the trajectory to quantify the instantaneous drop velocity (data not shown).

It is evident from the images in Fig. 5a as well as the trajectories that the spacing between drops is reduced in the bypass channels as the drops move further into the network (see Movie S1, ESI†). This crowding of drops in the bypass channels is also apparent in Fig. 3b and c. In general, we observe that when an empty loop is present, the first (leader) drop enters the bypass channel and its velocity is reduced by 50% due to the carrier fluid leaking through the trap channel; causing it to slow down. While the leader drop is still in the bypass, the second (follower) drop in the main channel is moving at the original velocity of the train, effectively catching up with the leader drop. The interdrop distance between the leader and follower drop is thus reduced by 50%. Until unless parking occurs the spacing between the leader and follower drops progressively decreases causing crowding. When a parking event occurs, a large separation is introduced between neighboring drops, which is also reduced after traversing additional loops leading to crowding. Interestingly, we find that drops traversing the loop(s) already containing parked drop(s) move at nearly the original velocity of the train implying the parked drop confers high hydrodynamic resistance to the trap channel.

The above mechanism is the main cause of crowding and is particularly exemplified by drops with indices 1 and 6 in Fig. 5b, where despite the large initial separation they come close to each other. A direct consequence of crowding in this experiment is the astonishing sequence in which drop parking occurs: drop index = 4, 3, 5, 2, *etc.* (see the sequence in which trajectories flatten in Fig. 5b). It is also evident from Fig. 5b that the leader drop never gets parked in the network.

The crowding of confined drops in the bypass channels due to the collective hydrodynamics is the principal cause of

droplet collisions. We find that in majority of the tested flow conditions, crowding often brings the confined drops in close proximity. When coupled with the waiting times at the loop junctions, this proximity causes the follower drop to collide with the leading drop promoting confinement-guided break-up. Thus, crowding of drops in MPNs is an intrinsic feature of the network topology, inevitably promoting droplet collisions and generating polydisperse SDAs over a large control parameter space.

3. Influence of control parameters on parking modes and polydispersity of SDA. From our observations of the different parking modes, it appears that three control parameters control the collective dynamics in MPNs. First, is the non-dimensional drop volume V_d/V_T, which represents the ratio of volume of the primary drops in the train with the trap volume. This is an important parameter because the discrete parking mode (P1) and the parking due to collision-induced break up (P2) occur mostly when $V_d/V_T \sim O(1)$. In contrast, drop parking due to flow-induced breakup (P3) occurs for $V_d/V_T > 1$.

Second, is the spacing between the drops in the train, λ, which regulates the number of drops that can occupy the bypass channel and therefore the collective hydrodynamic feedback for drop parking. Thus, another control parameter is λ/L_B where L_B is the length of the bypass channel. Note that L_B would also be indicative of the maximum drop spacing in the train such that a drop exits the parking loop, just when the preceding one enters the loop. At this critical drop spacing, no collective interactions will occur.

The final control parameter is the capillary number, $Ca = \mu U/\gamma$, where μ is the viscosity of the carrier fluid, U is the sum of the two fluid phase velocities, and γ is the interfacial tension. Prior works[28,30,31] at simpler bifurcations than ours have shown that the competition between viscous and interfacial forces captures the break-up and coalescence behavior in confined microfluidic drops. We therefore used Ca as another control parameter.

Fig. 6 shows the impact of the three control parameters on the modes of parking and polydispersity with the dominant mode being highlighted in the legend. It is evident that P2 mode dominates the control parameter space. Generally, we find that collision-induced drop break up occurs for both $V_d/V_T > 1$ as well as $V_d/V_T < 1$, over the explored capillary number range and droplet spacing (see Fig. 6a and b). It is not very sensitive to initial drop spacing (Fig. 6a) because droplet crowding inevitably occurs despite droplets entering the MPN well separated (*c.f.* Section II.A.2). Interestingly, we observe from Fig. 6c that the polydispersity of the array is extremely large (more than 40%) especially when $V_d/V_T > 1$, while it is moderately high (between 5–40%) when $V_d/V_T < 1$. This is because, although collisions still occur when $V_d/V_T < 1$, breakup can be avoided due to the slipping of the smaller-sized drops at the junction.

We observe that P1 mode of parking exclusively occurs in the MPN when $V_d/V_T \leq 1$, and for large initial drop spacing, $\lambda/L_B \approx 0.5$, and very low Ca ≈ 0.001 (Fig. 6a and b). The large initial drop spacing prevents drops from coming into close contact even though the train moves through several loops. In addition, the small drop size and low capillary number mitigates break-up despite some close encounters between droplets. Thus, small drop size, large λ/L_B and low Ca essentially delays droplet collision-induced break-up in the finite 60-trap array investigated in the experiments. However, it is possible that as the size of the array increases, the droplet crowding mechanism (discussed in Section II.A.2) may eventually cause droplet break-up.

We do not have substantial conditions where P3 mode dominates, but it is expected that flow-induced breakup occurs

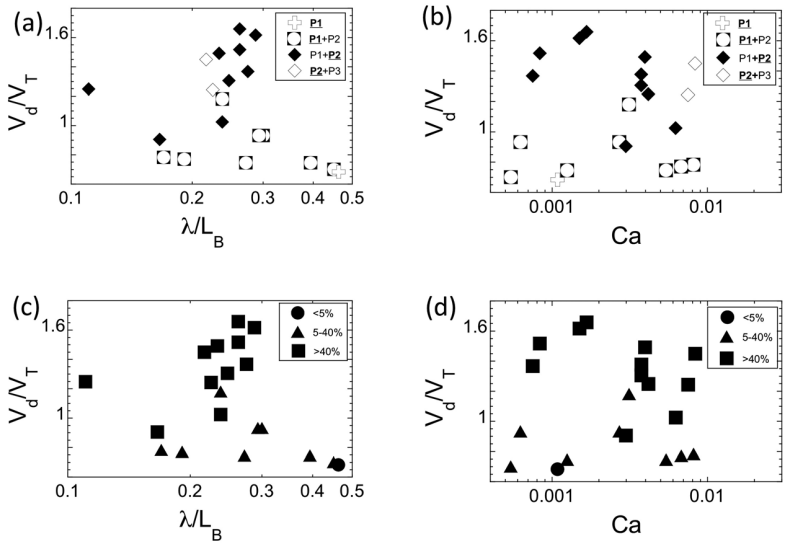

Fig. 6 Control parameters affecting the parking modes and polydispersity of the SDA, when using non-coalescing drops. (a, b) Influence of the non-dimensionalized drop volume (V_d/V_T), drop spacing (λ/L_B) and capillary number (Ca) on the parking modes. The frequently occurring mode of drop parking is indicated as bold and underlined in the legend. (c and d) Influence of the non-dimensionalized drop volume, drop spacing and capillary number on the polydispersity of the SDA. The legend shows the measured polydispersity.

when $V_d/V_T > 1$ and capillary number is high (≥ 0.01). The large capillary number is also prerequisite for confined droplet breakup in other bifurcation geometries suggesting that the regime for Ca $\geq$ 0.01 is dominated by flow-induced break-up and potentially drop squeezing.

B. Collective dynamics of coalescing drops

We studied the collective hydrodynamics of confined drops in the same 60-trap MPN, but with no surfactant added in the continuous phase. As shown in Fig. 7, most strikingly the SDA contained exceptionally monodisperse SDAs over a broad range of flow conditions. In addition, the squeeze-through limit is pushed to higher flow rates ($Q_o > 1000$ μL h^{-1}) due to the higher interfacial tension of the surfactant-free drops.

1. Modes of parking. In Fig. 8 we show the instantaneous snapshots of the dynamics of coalescing drops for a representative flow condition (see Movie S2, ESI†). We find that the exceptional monodispersity in the array was due to a stunning manifestation of complex collective behavior that led to rectification of polydispersity in drop volumes. As shown in Fig. 8a, if the trap is overfilled due to parking of a larger primary drop *via* P1 mode, the overfilled volume gets rectified by a subsequent drop through coalescence and break-up. Likewise, as shown in Fig. 8d, if the trap is underfilled, for example due to collision-induced break-up (see Fig. 8c), then a subsequent drop in the train coalesces with the underfilled drop and breaks as it passes through the bypass channel, rectifying the fluid volume in the trap. Fig. 8e shows that the passing drops flowing through the network continue to coalesce with the trapped drops ensuring exceptional uniformity of parked drops. Collectively, we refer to these mechanisms of rectifying drop volumes as hydrodynamic self-rectification.

In general, we find that the three parking modes P1, P2 and P3 also can occur with the surfactant-free drops, similar to the case of non-coalescing drops. For example, Fig. 8b and c show the P3 and P2 parking modes with coalescing drops respectively. However, the ability of drops to coalesce yields a new collective mode of parking.

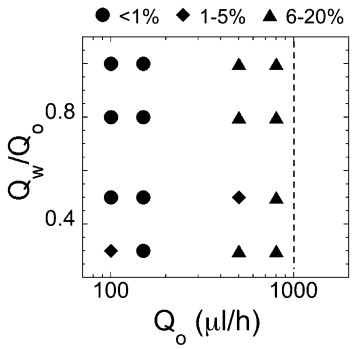

Fig. 7 The flow conditions tested for drops without added surfactant in the continuous phase. The legend denotes polydispersity in drop volumes in the array. The dashed vertical line indicates the approximate onset of squeezing of the drops through the traps.

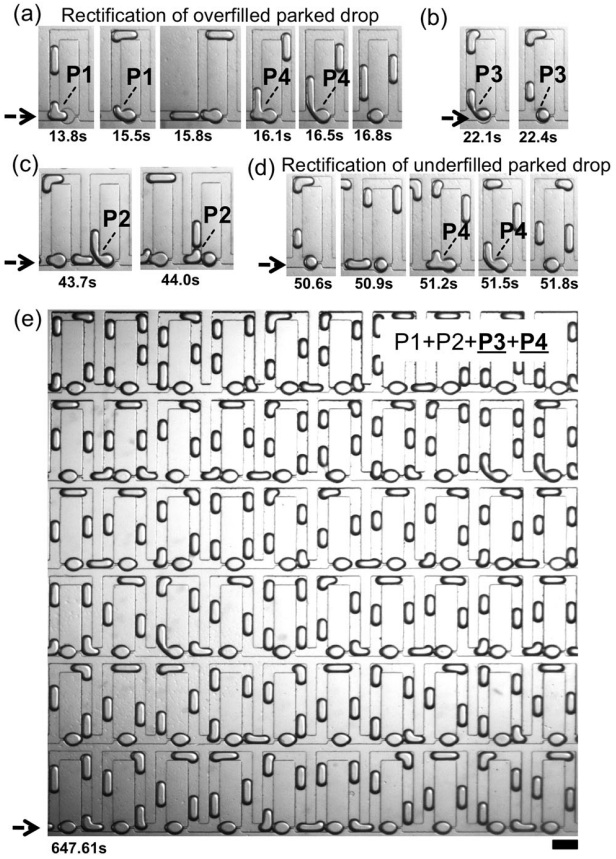

Fig. 8 Time-stamped image sequence showing the collective dynamics of coalescing drops in the MPN. (a) Rectification of the volume of an overfilled trapped drop due to parking modes P1 and P4. (b, c) Parking modes P3 and P2 also occur with coalescing drops. (d) Rectification of the volume of an underfilled drop (which resulted from P3 mode of parking) by P4 mode of parking. (e) Final monodisperse SDA resulting from the use of coalescing drops in the MPN. All the four modes of parking (P1 + P2 + P3 + P4) are involved in the hydrodynamic self-rectification process. Q_o = 100 μL h^{-1} and Q_w/Q_o = 0.3. The dashed arrows indicate the flow direction. Scale bar is 500 μm.

P4 – drop parking due to break-up of coalesced drops. We find that similar to the non-coalescing drops, crowding also occurs with surfactant-free drops. This crowding causes not only the primary but also the fragmented drops to coalesce at either the loop junction or at the turns in the bypass, causing them to be longer, as shown in Fig. 8a and d. These longer coalesced drops undergo parking by break-up at the junction, similar to the P3 parking mode. Thus, although P1, P2 and P3 collective modes also exist in the coalescing drop experiments, the emergence of P4 mode of parking together with the hydrodynamic self-rectification mechanisms cause the droplet arrays to be monodisperse.

2. Influence of control parameters on parking modes and polydispersity of SDA. To understand the collective dynamics of the coalescing drops over a broad range, we conducted additional experiments, than those depicted in Fig. 7. In the additional experiments, we not only pursued a wider range of the water to oil flow rate ratio (Q_w/Q_o) but also used auxiliary side-channels downstream of the drop generator to change the

Capillary number (Ca) and droplet spacing (λ) while maintaining the drop volume constant. We use the same three control parameters (V_d/V_T, λ/L_B and Ca) as the non-coalescing drops and report the influence of these parameters on modes of parking modes and polydispersity of the SDA.

As shown in Fig. 9a and b we identify approximately three regimes depending on which parking modes dominates. These regimes depend largely on the drop volume ratio, V_d/V_T, and are insensitive to the capillary number and drop spacing in the train. In the first regime characterized by $V_d/V_T < 1.2$, we find both P1 and P4 modes acting with P1 being the dominant mode of parking. In the second collective regime, $1.2 < V_d/V_T < 2.3$, the drop parking in the network is dominated by the parking modes P3 and P4 because the drops are larger than the traps. However, some underfilling and overfilling events also occur due to modes P1 and P2. In the third collective regime, $V_d/V_T > 2.3$, the primary drops are long, resulting in modes P3 and P4 dominating the parking, with very few occurrences of under filling due to mode P2.

In Fig. 9c and d we map the polydispersity of the SDA for all the flow conditions tested as a function of dimensionless drop volume, drop spacing and capillary number. We find that the polydispersity does not correlate well with drop spacing since monodisperse and polydisperse SDAs exist for the same λ/L_B values (Fig. 9c). The polydispersity of the SDA correlates better with capillary number, with monodisperse arrays being observed for $Ca < 0.002$ and polydisperse arrays for $Ca > 0.002$ (Fig. 9d). Thus, $Ca = 0.002$ represents the threshold for hydrodynamic self-rectification to take place, and the regime of self-rectification is defined by $V_d/V_T > 1.2$ and $Ca < 0.002$.

III. Discussion

Development of methods to trap arrays of droplets of defined size in microfludic devices is important for a variety of material science (*e.g.* nucleation and phase behavior) as well as biological (*e.g.* single cell analysis) applications. Current approaches[11–13,32–40] to produce SDAs often require simultaneous optimization of drop production (*e.g.* drop size and spacing), surfactant concentration (*e.g.* to avoid drop coalescence), obstacle geometry (*e.g.* trap size, groove width), network architecture (*e.g.* placement of traps/grooves) and flow conditions (*e.g.* to prevent drop dislodging). Some of these limitations of current SDA methods are evident from this study when using non-coalescing droplets in MPNs. Drop size in the train needs to be commensurate with the trap size as well as drop spacing needs be tuned to induce the desired hydrodynamic feedback – which can be difficult due to start-up effects and flow rate fluctuation in syringe pumps. Thus, the droplet production and MPN geometry needs to be tightly controlled when a train of non-coalescing droplets is used to produce SDAs.

The limitations of non-coalescing droplets in MPNs can be resolved by injecting a single long immiscible plug as shown by us and others.[11,15,17] The long plug then traverses sequentially through each parking loop, filling the trap and breaking-off at the junction; ultimately yielding a highly monodisperse droplet array. As a result, the long-plug method does not require the need to tune drop size to trap size. However, the long-plug method suffers from two limitations. First, as the number of traps in the SDA increases, much longer plugs need to be injected. Such extremely long plugs may fragment at undesired

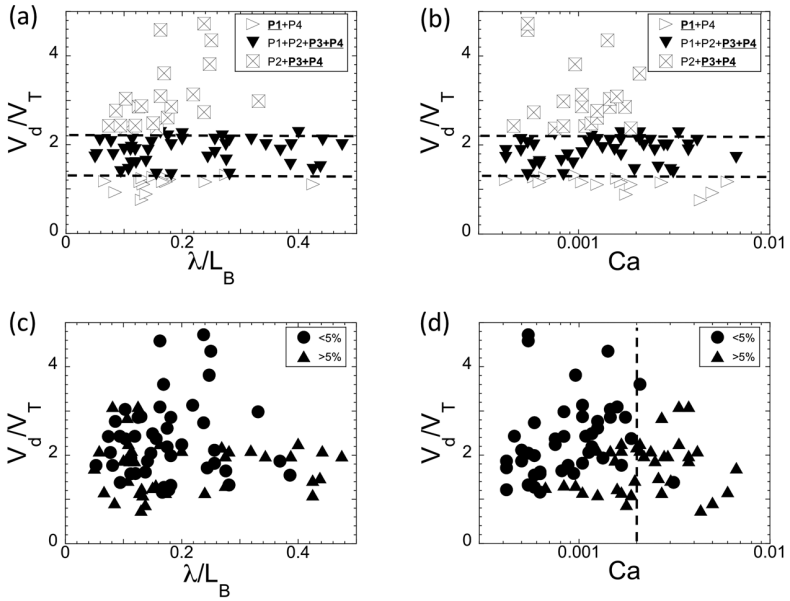

Fig. 9 Control parameters affecting the parking modes and polydispersity of the SDA, when using coalescing drops. (a and b) Influence of the non-dimensionalized drop volume (V_d/V_T), drop spacing (λ/L_B) and capillary number (Ca) on the parking modes. The dashed horizontal lines highlight the three different collective behaviors based on drop parking modes. (c and d) Influence of the non-dimensionalized drop volume, drop spacing and capillary number on the polydispersity of the SDA. The legend shows the measured polydispersity. The dashed vertical line in (d) highlights the threshold capillary number for hydrodynamic self-rectification.

locations in the network due to interfacial instabilities or wetting defects in the network. In addition, if multiple long plugs are injected, their size and spacing still needs to be tuned. Second, as we demonstrated recently[14,15] when long plugs containing non-Brownian microparticles or cells are injected, the particles/cells may sediment during the long residence time of the plug in the network, eventually accumulating at the tail of the plug. As a result, droplet arrays containing highly non-uniform distribution of particles/cells are produced by the long-plug method.

In this study we demonstrate that injecting a train of coalescing drops into the MPN yields highly monodisperse SDAs when $V_d/V_T > 1$ and Ca < 0.002. Since this rectification window is large, the use of coalescing drops in MPNs addresses the limitations of both the non-coalescing drops as well as the long-plug method. Drop production need not be tightly controlled, *i.e.* highly monodisperse SDAs can be produced despite non-idealities in syringe pump-driven droplet generation. In addition, coalescing drops that are sufficiently small can be generated and their residence time in the network can be tuned to avoid particle sedimentation effects and non-uniform distribution of particles/cells in SDAs.[14] Thus, coalescing drops in MPNs provide a highly flexible method for creating monodisperse SDAs.

In addition to creating SDAs of uniform-sized droplets, coalescing drops provide other benefits that are difficult to achieve by current SDA methods. As shown in Fig. 10a droplet arrays with bimodal distribution can be obtained due to occurrence of the P1 parking mode at the beginning of the array and P4 parking mode downstream of the network. This result was obtained by injecting a train with primary drop volumes slightly smaller than the trap volume. The primary drops are parked in the first three rows of the MPN due to P1 mode of parking. However the passing drops coalesce further downstream due to the crowding mechanism (*cf.* Section II.A.2) and these longer coalesced drops fill the trap much more than the primary drops; causing a bimodal distribution. Thus, by controlling which mode operates when in the network, it is possible to achieve diversity in drop size distribution.

Instead of passively programming the parking modes in the network, a much tighter control of drops volumes can be achieved *via* hydrodynamic self-rectification by hard-wiring the trap dimensions. As shown in Fig. 10b, SDAs of tunable drop volumes can be produced by simply controlling the dimension of the trap in a single MPN network or by connecting in series MPNs containing distinct trap sizes (Fig. 10c). Since the hydrodynamic self-rectification process is independent of drop volume and spacing in the train, in both cases, drop volumes can be stored that are commensurate with trap volume. Such flexibility is virtually impossible to achieve with current methods of generating SDAs.

The self-rectification phenomenon has the potential to deliver additional control for manipulating SDAs, than demonstrated here. We observed that above the critical capillary number Ca > 0.002 rectification was not efficient. We recently explained the origin of this limit in Ca (see Fig. 4 in ref. 14). When operating beyond this critical capillary number, the parked drop deforms significantly due to the increased fluid stress from the continuous phase. The significant deformation of the parked drop at high Ca blocks the constriction in the trap, resulting in less continuous phase flow leaking through the trap channel. Therefore passing drops at high Ca do not penetrate deeply enough into the trap for coalescence to occur with the parked drop, making rectification less favorable. This threshold in capillary number can be exploited as a switch to make specific droplets in a train to coalesce with droplets already parked in the SDA by modulating in time the velocity of the droplet train. Achieving such fine control at the level of

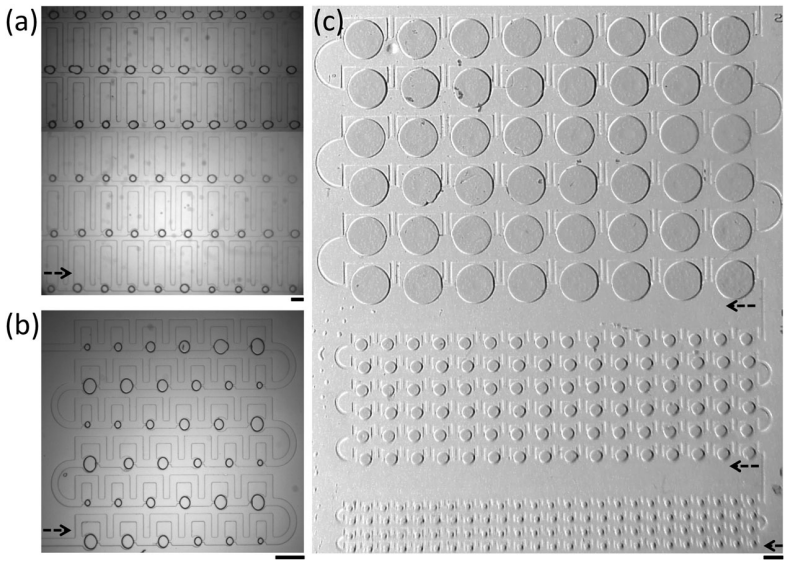

Fig. 10 Hydrodynamic self-rectification provides flexible control over drop volumes in SDAs. (a) Droplet array with biomodal drop volume distribution of 10 and 16 nL. (b) Array with variable drop volume (2–25 nL). (c) Three MPNs connected serially produce droplet arrays with volume 2, 20 and 200 nL. The dashed arrows indicate the flow direction. Scale bar is 1 mm.

individual droplets can enable coalescence-induced transfer of cargo (reagents or particles) between moving droplets and specific parked droplets in the SDA.

IV. Conclusions

In this study, we document in detail the collective dynamics of trains of surfactant-covered and surfactant-free drops in MPNs. For both these systems, we identify different parking modes and characterize their impact on the polydispersity of the SDA. We also map how system control parameters affect the modes of parking and polydispersity. We find that, in contrast to non-coalescing droplets, coalescing droplets provide a much more simpler and flexible means to create SDAs of monodisperse parked drops as well as droplet arrays with user-defined parked droplet volumes. In fact, our findings suggest that coarse (polydisperse) emulsions made by shaking or stirring can be injected into large-scale MPNs to create user-defined emulsions on the device.

Our results show that droplets with no surfactant coverage can be arrayed at prescribed coordinates in a microfluidic device. The presence of a bare interface with the coalescing-drop approach may pose undesirable interfacial transport issues in applications where droplets need to be used as microreactors, however it offers significant utility in other areas. For example, the well-defined initial condition of a bare interface allows flow-based delivery of interfacially active materials (*e.g.* surfactants, proteins, lipids and nanoparticles) at specified time points lending to precise control and decoration of interface on an ensemble of droplets with tunable surface-to-volume ratio. Such a novel capability can be used to fundamentally investigate a variety of interfacial phenomena including kinetics of surfactant or particle adsorption,[41] competitive displacement of proteins by small-molecule surfactants[42] and mechanics of decorated droplets based on their flow-induced squeezing dynamics.[43]

V. Materials and methods

Fabrication of MPNs

In our experiments, unless otherwise specified, we fabricated MPNs containing 60 traps using soft lithography.[44] Polydimethyl siloxane (PDMS) prepolymer and curing agent were mixed in a 10 : 1 ratio, degassed and poured on the mold and cured for a minimum of two hours at 65 °C. Subsequently the PDMS replica was cut with a scalpel and peeled. Inlet and outlet reservoirs were defined by punching holes. The replica was placed on a PDMS coated glass slide that was partially cured in the oven at 65 °C for 10 minutes. The entire assembly was further cured at 65 °C for two hours to create an irreversible seal. The device has R_T/R_B = 1.5 and channel height, H = 200 μm. The trap diameter, D = 320 μm and the width and length of the constriction preventing drop squeezing is w_c = 40 μm and l_c = 100 μm respectively. The width of the channel containing the drop train as well as the bypass is W = 200 μm. The bypass length, L_b = 4000 μm.

Microfluidic experiments

Given that the resistance of the MPN increases (and fluctuates) as droplets are produced and enter into the network, we chose to conduct all our experiments using constant flow-rate sources rather than constant-pressure sources. Trains of monodisperse confined drops are injected into the MPN by controlling the aqueous (Q_w) and oil (Q_o) flow ates at an upstream T-junction using syringe pumps (PHD2000, Harvard Apparatus). We fabricated devices in PDMS using soft lithography, where all the four walls of the channel are made of PDMS ensuring uniform wettability of the continuous phase. We used embryonic mineral oil (Sigma Aldrich, Part # M5904, viscosity, μ_c = 30 mPa.s) as the continuous phase, and this oil has very good wettability with PDMS.[45] The dispersed phase is water. We explore two limiting cases of surfactant (Span 80) concentration: 0 and 2 wt%, the former enables drops to merge during collisions and the latter prevents coalescence. Both the capillary number (Ca) and Reynolds number (Re) corresponding to this study are <0.01. Here Ca = $\mu_c U/\gamma$ and Re = $\rho_c Uh/\mu_c$, where ρ_c and U are the density of the oil phase and the total mean velocity respectively, and γ (=50 mN m^{-1} for no surfactant and 5 mN m^{-1} with 2 wt% Span 80) is the interfacial tension. In this study, the range of velocities of the droplets is 0.75–8.44 mm s^{-1}. The frequency of droplet formation in our experiments ranges 24–480 drops/min, and the droplet trapping frequency in the array is 8–90 drops per min.

Experiments were conducted on a stereo microscope (SZX16, Olympus). Experimental movies were recorded using high speed camera (PCO1200, Cooke Corp, MI).

Data analysis

All images and movies were analyzed using Image J v.1.43r. The volume of drops in the train (V_d) was calculated by measuring the length of the drop and then multiplying by the width and height of the channel. This method of calculating V_d yielded values that are within 2% of the values of V_d that would be obtained by taking the ratio of aqueous flow rate and droplet frequency. The trapped drop volume was calculated by multiplying the projected area of the droplet with the height of the device. We compared the trapped drop volume for the discrete drop parking (P1) case where there was no breakup of the droplet in the train with the drop volume in the train (V_d) and found the variation is less than 1.5%, indicating that our approach of determining V_T is accurate. Polydispersity is reported as a percentage of the coefficient of variance of trapped drop volumes in the array. Droplet array was considered to be monodisperse when the polydispersity was $<5\%$.

Acknowledgements

We acknowledge the National Science Foundation (CAREER: 1150836) for supporting this work, and Kim Jihye for producing Fig. 10c.

References

1 G. F. Christopher and S. L. Anna, Microfluidic methods for generating continuous droplet streams, *J. Phys. D: Appl. Phys.*, 2007, **40**, R319.

2 S. Ralf, B. Martin, P. Thomas and H. Stephan, Droplet based microfluidics, *Rep. Prog. Phys.*, 2012, **75**, 016601.

3 T. Beatus, R. H. Bar-Ziv and T. Tlusty, The physics of 2D microfluidic droplet ensembles, *Phys. Rep.*, 2012, **516**, 103–145.

4 P. J. A. Janssen, *et al.*, Collective dynamics of confined rigid spheres and deformable drops, *Soft Matter*, 2012, **8**, 7495–7506.

5 M. J. Fuerstman, P. Garstecki and G. M. Whitesides, Coding/decoding and reversibility of droplet trains in microfluidic networks, *Science*, 2007, **315**, 828–832.

6 M. Schindler and A. Ajdari, Droplet traffic in microfluidic networks: A simple model for understanding and designing, *Phys. Rev. Lett.*, 2008, **100**, 044501.

7 W. Engl, M. Roche, A. Colin, P. Panizza and A. Ajdari, Droplet traffic at a simple junction at low capillary numbers, *Phys. Rev. Lett.*, 2005, **95**, 208304.

8 G. Cristobal, J. P. Benoit, M. Joanicot and A. Ajdari, Microfluidic bypass for efficient passive regulation of droplet traffic at a junction, *Appl. Phys. Lett.*, 2006, **89**, 034104.

9 M. Prakash and N. Gershenfeld, Microfluidic bubble logic, *Science*, 2007, **315**, 832–835.

10 J. Maddala, W. Wang, S. Vanapalli and R. Rengaswamy, Traffic of pairs of drops in microfluidic ladder networks with fore-aft structural asymmetry, *Microfluid. Nanofluid.*, 2013, **14**, 337–344.

11 H. Boukellal, S. Selimovic, Y. W. Jia, G. Cristobal and S. Fraden, Simple, robust storage of drops and fluids in a microfluidic device, *Lab Chip*, 2009, **9**, 331–338.

12 W. W. Shi, J. H. Qin, N. N. Ye and B. C. Lin, Droplet-based microfluidic system for individual *Caenorhabditis elegans* assay, *Lab Chip*, 2008, **8**, 1432–1435.

13 S. S. Bithi and S. A. Vanapalli, Behavior of a train of droplets in a fluidic network with hydrodynamic traps, *Biomicrofluidics*, 2010, **4**, 10.

14 S. S. Bithi, W. S. Wang, M. Sun, J. Blawzdziewicz and S. A. Vanapalli, Coalescing drops in microfluidic parking networks: a multifunctional platform for drop-based microfluidics, *Biomicrofluidics*, 2014, **8**, 034118.

15 M. Sun, S. S. Bithi and S. A. Vanapalli, Microfluidic static droplet arrays with tuneable gradients in material composition, *Lab Chip*, 2011, **11**, 3949–3952.

16 S. Selimovic, F. Gobeaux and S. Fraden, Mapping and manipulating temperature-concentration phase diagrams using microfluidics, *Lab Chip*, 2010, **10**, 1696–1699.

17 A. Dewan, J. Kim, R. H. McLean, S. A. Vanapalli and M. N. Karim, Growth kinetics of microalgae in microfluidic static droplet arrays, *Biotechnol. Bioeng.*, 2012, **109**, 2987–2996.

18 H.-H. Jeong, S. H. Jin, B. J. Lee, T. Kim and C.-S. Lee, Microfluidic static droplet array for analyzing microbial communication on a population gradient, *Lab Chip*, 2015, **15**, 889–899.

19 M. Belloul, W. Engl, A. Colin, P. Panizza and A. Ajdari, Competition between Local Collisions and Collective Hydrodynamic Feedback Controls Traffic Flows in Microfluidic Networks, *Phys. Rev. Lett.*, 2009, **102**, 194502.

20 D. A. Sessoms, A. Amon, L. Courbin and P. Panizza, Complex dynamics of droplet traffic in a bifurcating microfluidic channel: periodicity, multistability, and selection rules, *Phys. Rev. Lett.*, 2010, **105**, 154501.

21 J. Maddala, B. Srinivasan, S. S. Bithi, S. A. Vanapalli and R. Rengaswamy, Design of a model-based feedback controller for active sorting and synchronization of droplets in a microfluidic loop, *AIChE J.*, 2012, **58**, 2120–2130.

22 J. Maddala, S. A. Vanapalli and R. Rengaswamy, Origin of periodic and chaotic dynamics due to drops moving in a microfluidic loop device, *Phys. Rev. E: Stat., Nonlinear, Soft Matter Phys.*, 2014, **89**, 023015.

23 W. S. Wang and S. A. Vanapalli, Millifluidics as a simple tool to optimize droplet networks: case study on drop traffic in a bifurcated loop, *Biomicrofluidics*, 2014, **8**, 064111.

24 A. Schmit, L. Salkin, L. Courbin and P. Panizza, Cooperative breakups induced by drop-to-drop interactions in one-dimensional flows of drops against micro-obstacles, *Soft Matter*, 2015, **11**, 2454–2460.

25 J.-C. Baret, Surfactants in droplet-based microfluidics, *Lab Chip*, 2012, **12**, 422–433.

26 H. Wen, Y. Yu, G. Zhu, L. Jiang and J. Qin, A droplet microchip with substance exchange capability for the developmental study of *C. elegans*, *Lab Chip*, 2015, **15**, 1905–1911.

27 P. Garstecki, M. J. Fuerstman, H. A. Stone and G. M. Whitesides, Formation of droplets and bubbles in a microfluidic T-junction-scaling and mechanism of break-up, *Lab Chip*, 2006, **6**, 437–446.

28 G. F. Christopher, *et al.*, Coalescence and splitting of confined droplets at microfluidic junctions, *Lab Chip*, 2009, **9**, 1102–1109.

29 D. R. Link, S. L. Anna, D. A. Weitz and H. A. Stone, Geometrically mediated breakup of drops in microfluidic devices, *Phys. Rev. Lett.*, 2004, **92**, 054503.

30 L. Menetrier-Deremble and P. Tabeling, Droplet breakup in microfluidic junctions of arbitrary angles, *Phys. Rev. E: Stat., Nonlinear, Soft Matter Phys.*, 2006, **74**, 035303.

31 D. R. Link, S. L. Anna, D. A. Weitz and H. A. Stone, Geometrically mediated breakup of drops in microfluidic devices, *Phys. Rev. Lett.*, 2004, **92**, 054503.

32 A. Huebner, *et al.*, Static microdroplet arrays: a microfluidic device for droplet trapping, incubation and release for enzymatic and cell-based assays, *Lab Chip*, 2009, **9**, 692–698.

33 W. B. Du, L. Li, K. P. Nichols and R. F. Ismagilov, SlipChip, *Lab Chip*, 2009, **9**, 2286–2292.

34 C. H. J. Schmitz, A. C. Rowat, S. Koster and D. A. Weitz, Dropspots: a picoliter array in a microfluidic device, *Lab Chip*, 2009, **9**, 44–49.

35 Q. Q. Zhang, S. J. Zeng, J. H. Qin and B. C. Lin, Microfluidic droplet trapping array as nanoliter reactors for gas–liquid chemical reaction, *Electrophoresis*, 2009, **30**, 3181–3188.

36 M. Zagnoni and J. M. Cooper, A microdroplet-based shift register, *Lab Chip*, 2010, **10**, 3069–3073.
37 D. E. Cohen, T. Schneider, M. Wang and D. T. Chiu, Self-Digitization of Sample Volumes, *Anal. Chem.*, 2010, **82**, 5707–5717.
38 W. Wang, C. Yang and C. M. Li, On-demand microfluidic droplet trapping and fusion for on-chip static droplet assays, *Lab Chip*, 2009, **9**, 1504–1506.
39 P. Laval, N. Lisai, J. B. Salmon and M. Joanicot, A microfluidic device based on droplet storage for screening solubility diagrams, *Lab Chip*, 2007, **7**, 829–834.
40 P. Abbyad, R. Dangla, A. Alexandrou and C. N. Baroud, Rails and anchors: guiding and trapping droplet microreactors in two dimensions, *Lab Chip*, 2011, **11**, 813–821.
41 Y. He, P. Yazhgur, A. Salonen and D. Langevin, Adsorption–desorption kinetics of surfactants at liquid surfaces, *Adv. Colloid Interface Sci.*, 2014, DOI: 10.1016/j.cis.2014.09.002.
42 M. B. Munk, F. H. Larsen, F. W. J. van den Berg, J. C. Knudsen and M. L. Andersen, Competitive Displacement of Sodium Caseinate by Low-Molecular-Weight Emulsifiers and the Effects on Emulsion Texture and Rheology, *Langmuir*, 2014, **30**, 8687–8696.
43 S. Guido and V. Preziosi, Droplet deformation under confined Poiseuille flow, *Adv. Colloid Interface Sci.*, 2010, **161**, 89–101.
44 D. C. Duffy, J. C. McDonald, O. J. Schueller and G. M. Whitesides, Rapid Prototyping of Microfluidic Systems in Poly(dimethylsiloxane), *Anal. Chem.*, 1998, **70**, 4974–4984.
45 F. Malloggi, S. A. Vanapalli, H. Gu, D. van den Ende and F. Mugele, Electrowetting-controlled droplet generation in a microfluidic flow-focusing device, *J. Phys.: Condens. Matter*, 2007, **19**, 462101.

